



Article

# The Stability and Chloride Entrapping Capacity of ZnAl-NO<sub>2</sub> LDH in High-Alkaline/Cementitious Environment

Zahid M. Mir <sup>1,\*</sup>, Celestino Gomes <sup>2</sup>, Alexandre C. Bastos <sup>2</sup>, Rui Sampaio <sup>2</sup>, Frederico Maia <sup>3</sup>, Cláudia Rocha <sup>3</sup>, João Tedim <sup>2</sup>, Daniel Höche <sup>1</sup>, Mario G. S. Ferreira <sup>2</sup> and Mikhail L. Zheludkevich <sup>1,4</sup>

<sup>1</sup> Institute of Materials Research, Helmholtz-Zentrum Geesthacht Centre for Materials and Coastal Research, Max-Planck Str. 1, 21502 Geesthacht, Germany; daniel.hoeche@hzg.de (D.H.); Mikhail.Zheludkevich@hzg.de (M.L.Z.)

<sup>2</sup> DEMaC—Department of Materials and Ceramic Engineering, and CICECO—Aveiro Institute of Materials, Universidade de Aveiro, 3810-193 Aveiro, Portugal; jcv.gomes@ua.pt (C.G.); acbastos@ua.pt (A.C.B.); ruisampaio@ua.pt (R.S.); joao.tedim@ua.pt (J.T.); mgferreira@ua.pt (M.G.S.F.)

<sup>3</sup> Smallmatek—Rua dos Canhas, 3810-075 Aveiro, Portugal; frederico.maia@smallmatek.pt (F.M.); claudia.rocha@smallmatek.pt (C.R.)

<sup>4</sup> Faculty of Engineering, University of Kiel, Kaiserstrasse 2, 24143 Kiel, Germany

\* Correspondence: zahid.mir@hzg.de

**Abstract:** In this work, the ZnAl-NO<sub>2</sub> LDH (layered double hydroxide) is investigated as a possible additive for mitigating the chloride-induced corrosion of steel in reinforced concrete. The investigation focused on the stability and chloride binding capacity of this LDH in the pH range typical of cementitious materials. Until pH = 12.5 the material was stable and effective in capturing chloride ions from the surrounding aqueous environment. For higher pH, precisely that of hydrated cement, the LDH was partially dissolved and OH<sup>−</sup> preferentially entrapped instead of Cl<sup>−</sup>. These results suggested that ZnAl-NO<sub>2</sub> has excellent chloride entrapping capability at neutral pH, but this is reduced with increasing pH. However, when the LDH was incorporated into mortars, the chloride ingress was delayed, signifying that the dissolution of LDH leads to a secondary mechanism responsible for chloride capture.

**Keywords:** layered double hydroxide; corrosion; concrete; reinforcing steel; pH; chloride



**Citation:** Mir, Z.M.; Gomes, C.; Bastos, A.C.; Sampaio, R.; Maia, F.; Rocha, C.; Tedim, J.; Höche, D.; Ferreira, M.G.S.; Zheludkevich, M.L. The Stability and Chloride Entrapping Capacity of ZnAl-NO<sub>2</sub> LDH in High-Alkaline/Cementitious Environment. *Corros. Mater. Degrad.* **2021**, *2*, 78–99. <https://doi.org/10.3390/cmd2010005>

Received: 23 December 2020

Accepted: 18 February 2021

Published: 21 February 2021

**Publisher's Note:** MDPI stays neutral with regard to jurisdictional claims in published maps and institutional affiliations.



**Copyright:** © 2021 by the authors. Licensee MDPI, Basel, Switzerland. This article is an open access article distributed under the terms and conditions of the Creative Commons Attribution (CC BY) license (<https://creativecommons.org/licenses/by/4.0/>).

## 1. Introduction

The corrosion of steel in reinforced concrete affects infrastructures worldwide [1–3]. The cost of early repair and the reconstruction of these structures can lead to severe economic losses [4]. Concrete is a porous material [5], and aggressive species like chloride ions can pass through the concrete cover, until reaching the steel reinforcement, where they disrupt the steel native passive layer and initiate corrosion [6,7]. Innovative techniques are required to slow down the chloride ingress in concrete, delay the corrosion process and extend the service life of reinforced concrete infrastructures. Layered double hydroxides (LDHs) are a new class of concrete additives which can entrap aggressive anions from the environment and release selected anions (e.g., corrosion inhibitor) from their galleries. Potential applications include sequestration of chloride and carbonate ions in aggressive environments, which in turn can potentially prolong the service life of structures susceptible to corrosion. LDHs have gained attention in the recent years, due to their ion exchange properties, not only in concrete technology [8] but also in various branches of science and engineering [9], as a de-icing additive for asphalt roads [10], catalysis, [11], pharmaceutical applications [12], photochemistry [13], electrochemistry [14,15], biochemistry [16] and more.

Layered double hydroxides (LDHs), also known as “hydrotalcite-like” materials [9,17], can be synthesized by co-precipitation [18] of metal salts in alkaline medium, resulting in an ionic arrangement of positively charged brucite-like layers, together with anions

between the layers, to balance the charge. LDHs can be represented by the following generalized formula:  $[M(II)_{1-x}M(III)_x(OH)_2]^{x+}(A^{n-})_{x/n}mH_2O$ , with M(II) as divalent, M(III) as trivalent metallic cations and  $A^{n-}$  as the interlayer anion [17,19]. LDHs have the potential of intercalating external anions by exchanging them with the anions originally present in their galleries, as represented in Figure 1. This process is called the ion exchange process and is usually dominated by the order of ions in the selectivity series for LDH.

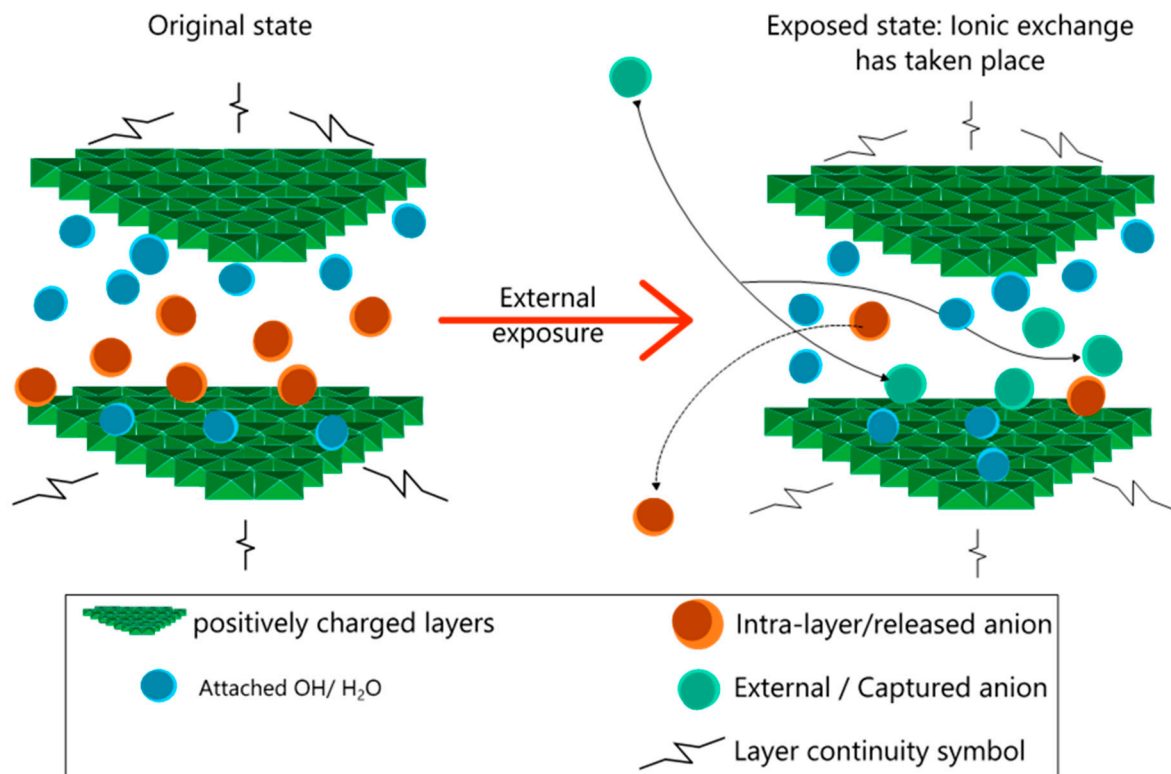


**Figure 1.** Schematic structure of layered double hydroxide (LDH) in original and exposed state and mechanism of ionic exchange.

Based on theoretical calculations, Costa et al. [20] concluded that Zn-Al-based LDHs have higher affinity to  $OH^-$  than  $Cl^-$ . They reported the anion selectivity order as  $CO_3^{2-} > OH^- > F^- > Cl^- > Br^- > NO_3^-$ . The ions towards the left of the series are preferable towards ion sequestration by LDH, as compared to the ions on the right of the selectivity series. Hibino [21] pointed out that such selectivity series for a particular LDH can change under certain conditions. Apart from the ion preference in the selectivity series, other factors, such as anion size, anion concentration and temperature, can influence the ion exchange process [8]. In cementitious materials, like cement paste, mortars or concrete, the ionic-exchange mechanism can be exploited to entrap chloride ions, thereby retarding their ingress, and simultaneously release anions with corrosion-inhibition properties, e.g.,  $NO_2^-$  [8,22]. If effective, this leads to a “self-protection” capability of concrete against corrosion of steel in concrete.

Earlier works on the use of LDH in cementitious environments include the controlled release of organic admixtures [23] and the acceleration of the hardening process with CaAl-Cl LDH [24]. Zhong et al. analyzed the chloride-binding capacity of MgAl LDH intercalated with  $CO_3^{2-}$  and  $NO_3^-$  and found higher capacity for the  $NO_3^-$  LDH type [25]. The effect of MgAl LDH on the microstructure and carbonation resistance of sulfoaluminate cement concrete was studied by Duan et al. [26]. In a separate study by the present authors [27], in situ XRD analysis revealed that MgAl LDH can possibly lead to the formation of higher amounts of AFm and thereby increase the chloride-binding capacity of concrete. Chen et al. [28] investigated the use of CaAl- $NO_3$  LDH for the removal of

chloride ions from concrete pore solutions and from cement paste. The sequestration of  $\text{Cl}^-$  ions was explained by an ionic exchange mechanism following a Langmuir isotherm in cement matrix. Similar Langmuir-type binding isotherms were also reported by Yoon et al. for the capture of chloride ions by on calcined MgAl-based LDH in cement paste [29]. A review of LDH as smart additives of reinforced concrete for anticorrosion applications was provided by Yang et al. [30]. Most of the LDHs tested so far in concrete belong to one of the following systems: MgAl or CaAl. Only a few papers exist with ZnAl LDH studied for the chloride capture and nitrite release in saturated  $\text{Ca}(\text{OH})_2$ , i.e., simulated concrete pore solution [31]. Additionally, a comprehensive review on the various types and applications of LDH in cementitious materials has recently been published by the authors [8].

As mentioned previously, the use of Zn-Al LDH in cementitious systems has not been extensively studied so far. Therefore, in this work, the authors studied the behavior and stability of ZnAl- $\text{NO}_2$  in depth. Additionally, this paper reflects on the results obtained in European Union's LORCENIS project [32], which focused on the ZnAl- $\text{NO}_2$  as a potential chloride-entrapping/corrosion-inhibiting additive for concrete. Due to these reasons, ZnAl- $\text{NO}_2$  system has been used in this paper.

In the present work, the authors focused on characterizing the working mechanism of ZnAl- $\text{NO}_2$  in high-alkaline environments typical to that of concrete and cement pastes. The broader goal of this study was to quantitatively and qualitatively assess the ion exchange process related to chloride ion capture by ZnAl- $\text{NO}_2$  in alkaline environments. The assessment is reported for aqueous salt solutions, as well as for pore solutions. A step-wise approach was followed in this study. At first, the LDH was exposed only to an environment containing  $\text{OH}^-$  anions, in order to verify its anion-capture capability, as well as its stability in alkaline environments. This was followed by exposing LDH to a multi-anionic environment, containing both  $\text{Cl}^-$  and  $\text{OH}^-$  ions. Moreover, the sequestration of each anion was evaluated, and the results are discussed in detail. Chloride-binding isotherms as a function of pH of the environment are also presented. Then the compatibility of the LDH with cement was analyzed by observing the effect of the LDH addition to cement paste in terms of the curing time. Furthermore, the chloride transport was monitored in mortars with LDH, by employing cast-in  $\text{Cl}^-$  sensitive sensors. Finally, the corrosion properties of steel embedded in mortars containing LDH are presented, in order to highlight the role of  $\text{NO}_2^-$  release from LDH (due to ion exchange or partial dissolution of LDH).

## 2. Materials and Methods

### 2.1. Material Synthesis

The Zn-Al- $\text{NO}_2$  LDH studied in this work was produced by Smallmatek, Lda, Aveiro, Portugal. It was prepared in a stainless-steel reactor, by co-precipitation of hydroxides from salts of divalent and trivalent cations, in a solution with an excess of sodium nitrite, and the pH adjusted to  $10.0 \pm 0.5$  with sodium hydroxide. More details can be found in Reference [33]. The resulting slurry was washed with deionized water, filtered and dried with an industrial spray dryer, to guarantee uniform and fine powder.

### 2.2. Materials Characterization

The LDH particle size was measured with a Coulter LS230 Particle Size Analyzer (Coulter Corporation, Miami, FL, USA). XRD diffractograms were obtained with a diffractometer PANalytical X'Pert MPD PRO (Almelo, The Netherlands) with Bragg-Brentano geometry, Ni-filtered  $\text{CuK}\alpha$  radiation, PIXcel<sup>1D</sup> detector, and step 0.026. The exposition was 2 s per step, in the angular range between  $3^\circ$  and  $65^\circ$ .

### 2.3. Stability of ZnAl- $\text{NO}_2$ in the High pH Range

The chemical stability of the LDH was analyzed at neutral pH and in the pH range from 11 to 13.5, which encompasses the pH of aged and fresh concrete. One gram of LDH was immersed in 50 mL of aqueous solutions with different pH values, prepared with distilled water and KOH. After 30 days in a closed container, the remaining powders were

washed, weighted by a lab scale and analyzed by XRD. The solution pH was measured by the potentiometric method with an Inlab Expert Pro pH combined electrode and a SevenMulti meter, both from Mettler Toledo (Columbus, OH, USA). The amount of  $\text{NO}_2^-$  in solution was measured with a UV-3100 UV-Vis-NIR spectrophotometer from Shimadzu (Kyoto, Japan), with the detection peak of interest occurring at 354 nm. Prior to the experimentation, the spectrophotometer was repeatedly calibrated by relating the intensity against various concentrations of  $\text{NO}_2^-$  in the calibration solutions.

#### 2.4. Chloride Binding Capacity

The chloride-binding capacity of ZnAl- $\text{NO}_2$  was studied with NaCl solutions ranging from 0.01 to 0.5 M at neutral pH, and then with pH from 11 to 13, following the test matrix shown in Figure 2. The tests were extended to leached pore solution extracts, in order to replicate a multi-ion competition scenario. Leached pore solution 1 (PS1) was made by mixing 3.5 g of ordinary Portland cement and 1.5 g of fly ash in 1 L of water, stirring for 24 h and allowed to rest for 3 days. The resulting pH was around 12.0. Leached pore solution 2 (PS2) was prepared by adding 50 g of cement to 1 L of water, stirring for 24 h and allowing to rest for 3 days prior to testing. The resulting pH was around 12.5. For each solution, 50 mL was added to a beaker, and the chloride concentration measured with a DX235-Cl ion-selective electrode (Mettler Toledo) connected with a mercury/mercurous sulfate reference electrode to a SevenMulti meter (Mettler Toledo). After a few minutes of stable reading, 1 g of LDH was added to solution, under stirring, while the  $\text{Cl}^-$  concentration was monitored and pH measurements were carried out just before and after 5 min of LDH addition. The ion-selective electrode was calibrated against standard chloride solutions (0.001 M to 0.5 M), every time, prior to conducting measurements. The experimental setup is pictorially depicted in Figure 3. In some cases, the solid was recovered after 5 min of exposure and characterized by XRD. To verify the effect of time on the binding capacity, the  $\text{Cl}^-$  and pH measurements were repeated after 15 days of the LDH addition.

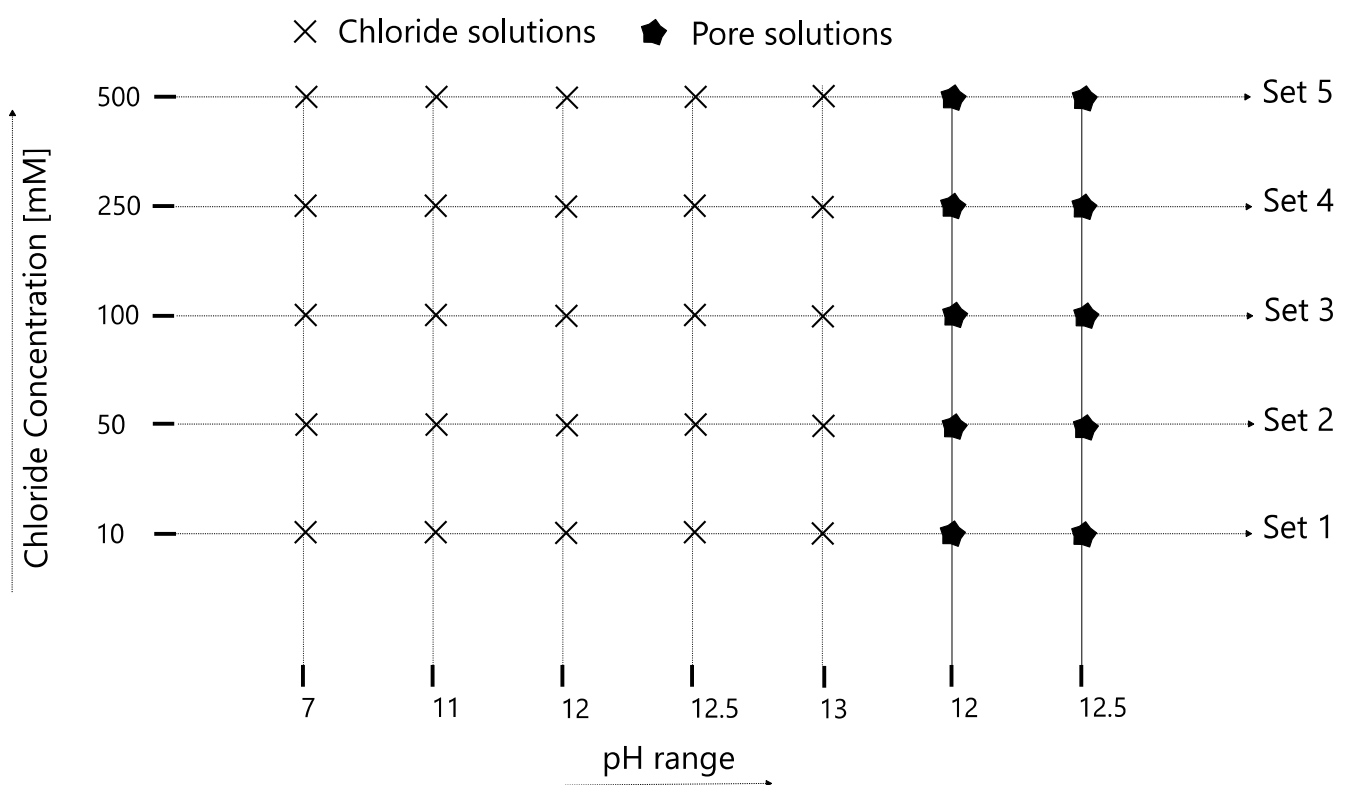
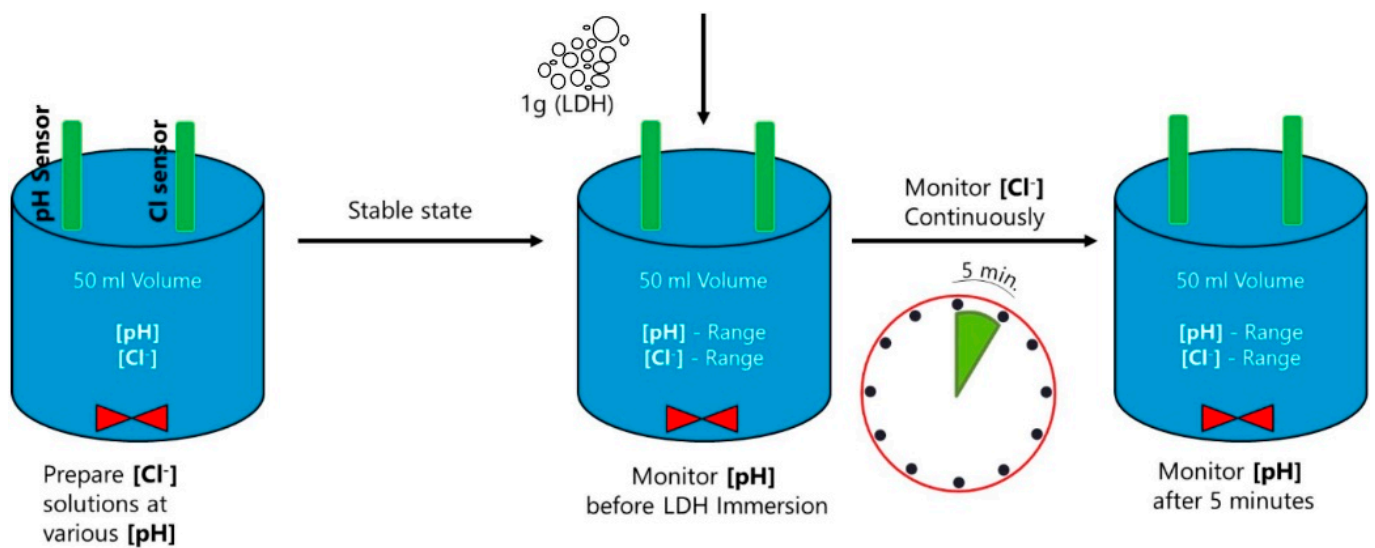


Figure 2. Test matrix for chloride-binding tests.



**Figure 3.** Experimental sequence for measuring  $\text{Cl}^-$  in the binding tests.

### 2.5. Compatibility of LDH with Cement Paste

Cement pastes with 0.5 water-to-cement (w/c) ratio were prepared without (reference) and with 2 wt% LDH. Specimens with  $30 \times 30 \times 10 \text{ mm}^3$  were cast and cured in a humidity chamber.

### 2.6. Chloride Sensors Embedded in Mortars

The effect of LDH on the chloride ingress in mortars was assessed with embedded chloride sensors. The sensors consisted of 1 mm diameter silver wire, coated with silver chloride on the polished surface and encased in epoxy. The silver chloride coat was produced galvanostatically, with a constant current density of  $2 \text{ mA/cm}^2$ , for 30 min, in 0.1 M HCl. Three of these  $\text{Cl}^-$  sensitive sensors were placed at 0.5, 1 and 1.5 mm from the surface of the mortar samples (Figure 4a). Prior to embedment in mortars, the sensors were calibrated by recording potential readings for various concentrations of  $\text{Cl}^-$  in  $\text{KOH} = 0.1 \text{ M}$  ( $\text{pH} \sim 13$ ). The response of the sensors to chloride ions in high-pH media is presented in Figure 4b. The chloride concentration in the mortars was then obtained by using the obtained calibration curve. These calibrations were repeated periodically, with sensors permanently immersed in  $\text{KOH} = 0.1 \text{ M}$  ( $\text{pH} \sim 13$ ), to certify that the response did not change with the continuous exposure to the alkaline environment of mortar.

The mortar samples were cast in  $5 \times 5 \times 5 \text{ cm}^3$  samples, with a composition of 14.5 wt% CEM II/B-L 32.5 N cement, 13% water and 72.5% of 0–2 mm size siliceous sand. The water/cement ratio was equal to 0.9 and was chosen for fast permeation and, consequently, to accelerate the chloride ingress. LDH was added in an amount corresponding to 2 wt% of cement (0.3 wt% of total mass of mortar). The mortar samples were cured for 28 days, in a humidity chamber, and then the samples were immersed in 3.5% NaCl aqueous solution. The potential of the sensors was measured against a saturated calomel electrode (SCE) placed in the external solution, using a CompactStat potentiostat connected to a peripheral differential amplifier (Ivium Technologies, Eindhoven, The Netherlands), for simultaneous measurement of several channels.

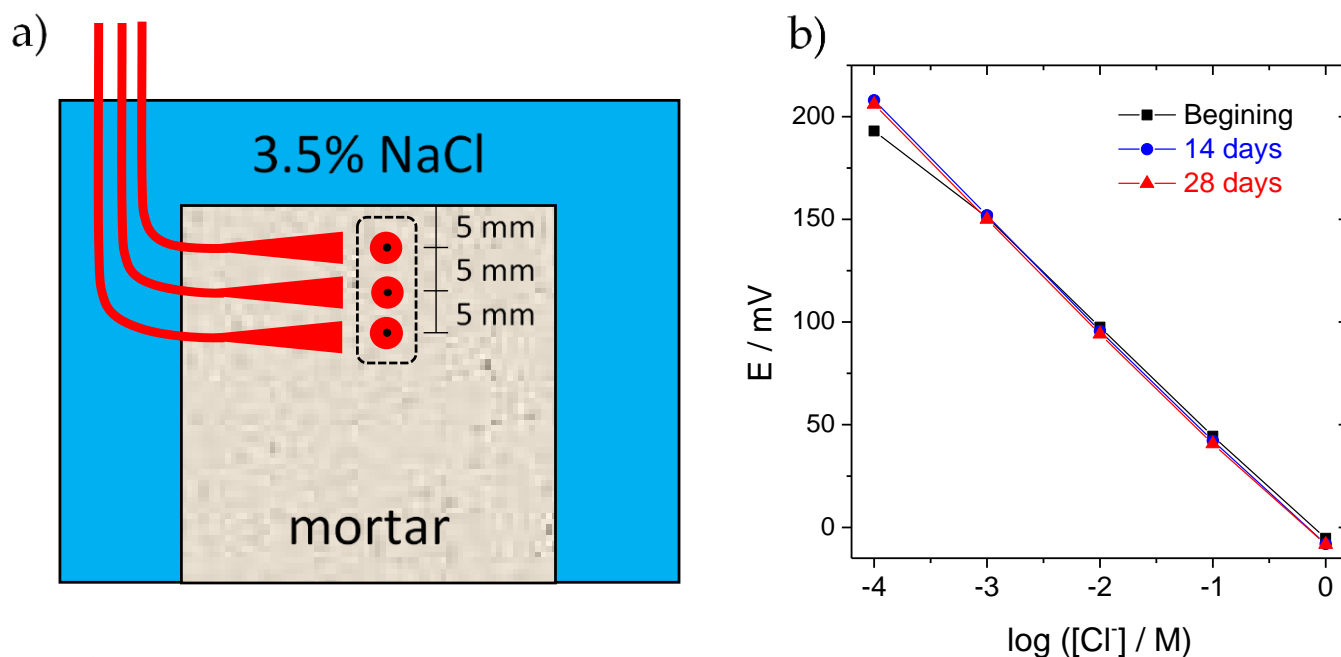


**Figure 4.** Studies conducted in mortars. (a) Scheme of mortar with sensors and (b) calibration curves for chloride sensors.

### 2.7. Corrosion Testing

Mortar samples with the composition presented in Section 2.6 and  $7 \times 4 \times 4 \text{ cm}^3$  size were produced, with a non-corrugated steel bar of 8 mm diameter placed in the middle. The steel bars were cleaned with 50% vol. HCl solution and abraded down to 1200 grade SiC paper, just before the embedment in the mortars. After 24 h, the samples were demolded and were left curing for 8 days, immersed in water. The samples were finally transferred to 3.5% NaCl solution, and the open-circuit potential and polarization resistance were measured periodically with a Autolab PGSTAT 204 potentiostat with a platinum counter electrode and a SCE electrode as reference. The polarization resistance was measured from  $-10$  to  $+10$  mV, with respect to the open-circuit potential, with a scan rate of  $0.1 \text{ mV s}^{-1}$ .

## 3. Results and Discussion

### 3.1. Characterization of the $ZnAl-NO_2$

The particle size distribution of the LDH powder is presented in Figure 5a. It ranged between 40 nm and 150  $\mu\text{m}$ , with a mean particle size of 22  $\mu\text{m}$ . Almost 10% of the particles exhibited a particle size of less than 5  $\mu\text{m}$ . The XRD pattern prior to exposure is depicted in Figure 5b and shows the reflections 003, 006, 110 and 113 at  $11.6^\circ$ ,  $23^\circ$ ,  $60.2^\circ$  and  $61.5^\circ$ . These reflections coincide with reflections reported in the literature for  $ZnAl-NO_2$  [31] and also with other LDHs with  $NO_2^-$  in the interlayer space [22,34].

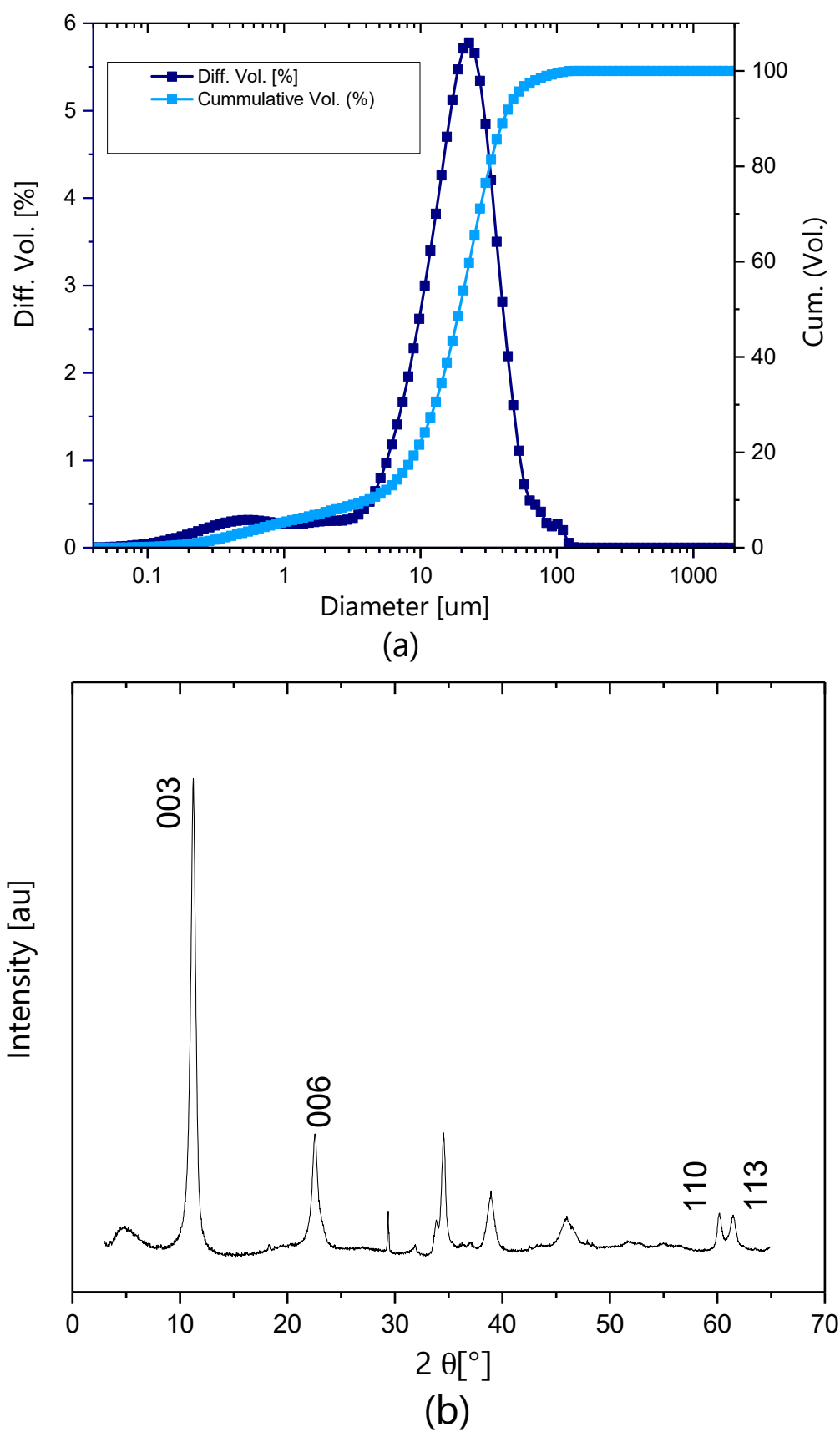


**Figure 5.** Characteristics of LDH particles. (a) Particle size distribution and (b) XRD pattern of ZnAl-NO<sub>2</sub> prior to exposure.

### 3.2. Stability in High-Alkaline Environment

The effect of pH in the range between 11 and 13.5 has been studied. The LDH and solution were analyzed 30 days after 1 g of powder was added to the 50 mL solution. After 30 days, the powders were extracted from the solutions and weighed. LDH powder was present in all samples. However, the amount of powder left at a high pH was less, indicating that a partial dissolution of LDH could have taken place. In a parallel experiment, it was verified that about 95% of solid remained undissolved at pH 12, decreasing to 60% at pH 13 and only 20% at pH 14. The pH of the solution just before and 30 days after the addition of LDH is presented in Figure 6a). The pH of the solutions inside the closed containers decreased noticeably. This was attributed to the capture of  $\text{OH}^-$  in solution by the LDH powder. A drop of three units in the pH scale was observed, showing a remarkable efficiency of this LDH to capture  $\text{OH}^-$ . For a higher pH, the amount of captured  $\text{OH}^-$  decreased (almost no pH drop), because most of the LDH was dissolved. The region of partial dissolution is marked in the figure.

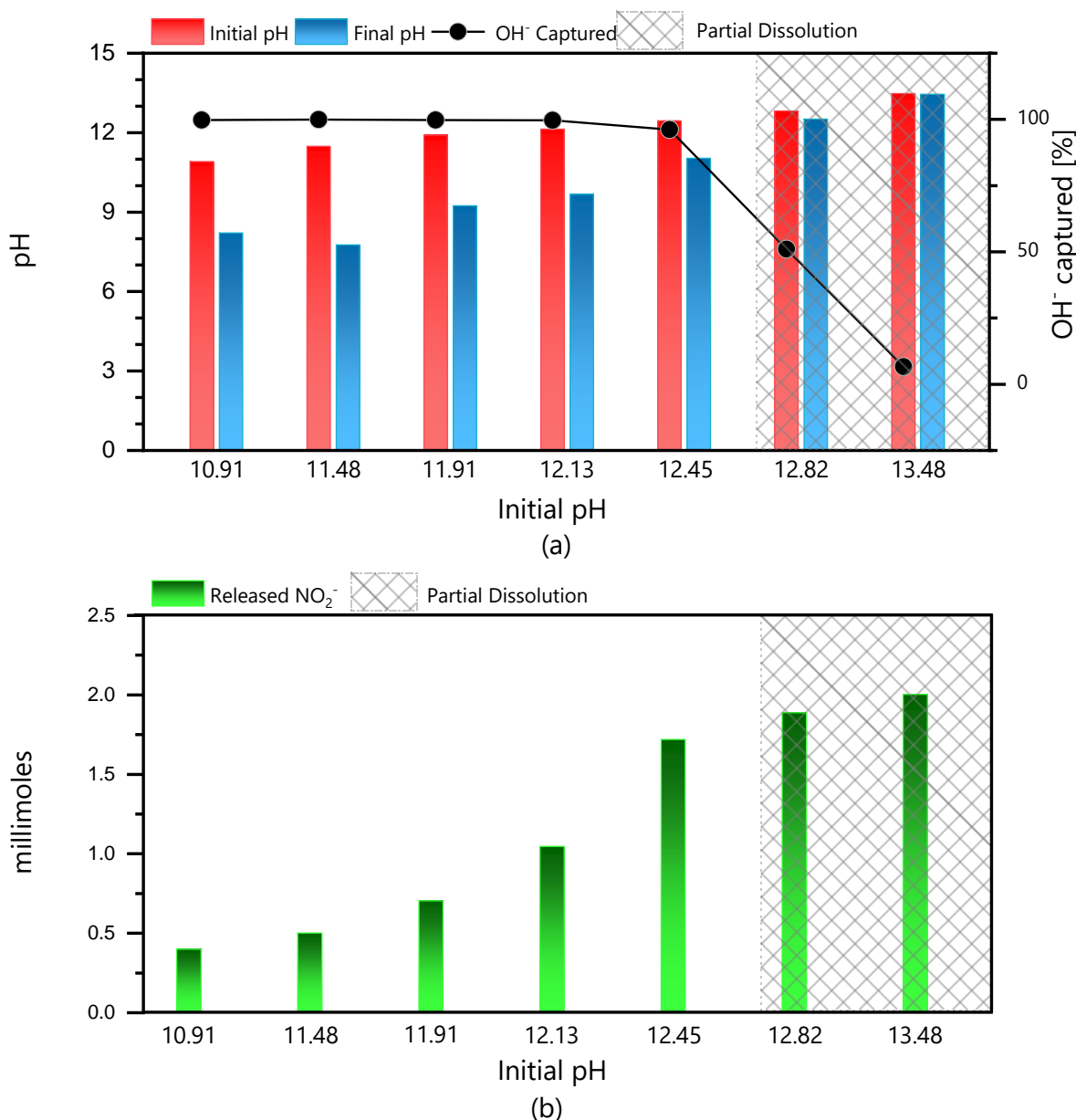


**Figure 6.** Stability and ion exchange property on LDH. (a)  $\text{OH}^-$  capture by LDH and in terms of pH drop and percent capture. (b) Corresponding  $\text{NO}_2^-$  release by LDH.

### 3.2.1. Release of $\text{NO}_2^-$ Ions

Considering that the capture of  $\text{OH}^-$  occurs by an ionic exchange mechanism, as expected for a LDH [9,15,17,22,23,30,31,33,34], the intercalated  $\text{NO}_2^-$  ions must leave the LDH interlayer and pass to solution, to allow the entrance of the incoming  $\text{OH}^-$  ions. Indeed, after 30 days of immersion,  $\text{NO}_2^-$  was detected in all the solutions. It was observed that the concentration of  $\text{NO}_2^-$  increased with an increase of pH, as shown in Figure 6b.

### 3.2.2. XRD Analysis of LDH Exposed to Alkaline Solutions

After the 30-day immersion period, the remaining powders were filtered, washed and dried in a vacuum oven, at 40 °C, for 24 h. Figure 7 shows the XRD patterns of the LDH before (base) and after immersion in the different solutions. The reflections 006 and 003 are related to basal planes while the peaks 110 and 113 correspond to non-basal planes. The magnification of the plot around the peak 003 ( $2\theta$  between 10° and 12°) shows a shift towards a higher angle as the pH increases, signifying a contraction of the interlayer.

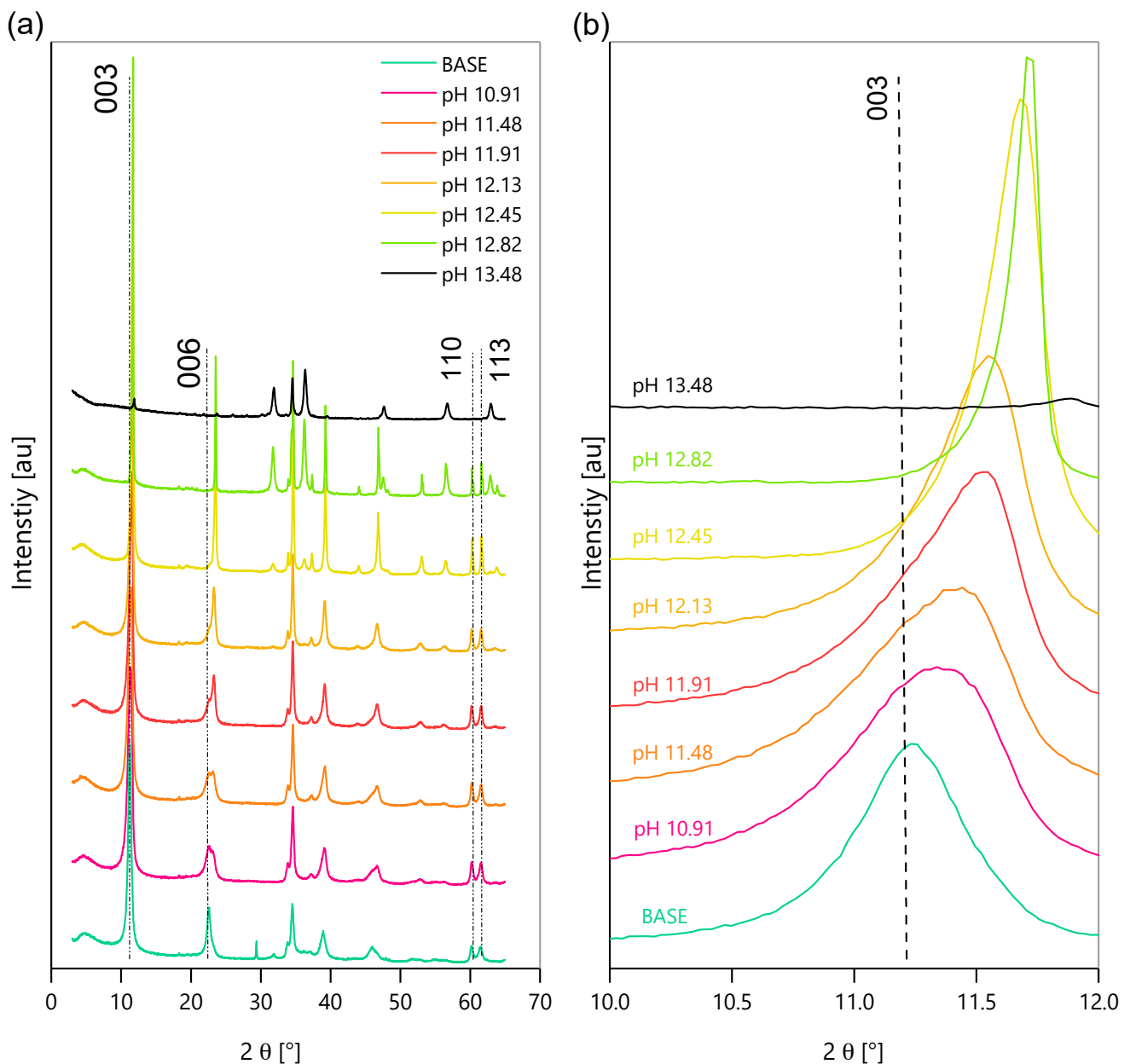


**Figure 7.** XRD analysis of ZnAl- $\text{NO}_2$  after 30 days of immersion in alkaline solutions—(a) Full XRD spectra (b) XRD spectra displaying  $d_{003}$  peaks.

Bragg's law [35] was used to calculate the interlayer spacings  $d_{003}$  and  $d_{110}$  from the  $2\theta$  peak locations, using  $\lambda\alpha = 1.540598 \text{ \AA}$ . The spacing  $d_{003}$  gives the thickness of a single brucite-like layer and one interlayer, while  $d_{110}$  is the distance between two-metallic cations in the brucite-like layer. A shift of  $d_{003}$  on the  $2\theta$  axis corresponds to a change in the interlayer distance, as observed in Figure 7b. In Figure 8, the calculated  $d_{003}$  and  $d_{110}$  values are plotted for each pH. A clear  $d_{003}$  shift to the right on the  $2\theta$  axis occurs as the pH increases, which is indicative of a smaller interlayer distance, signifying anion exchange with a smaller radius ion. The  $\text{OH}^-$  ion has a smaller size than the  $\text{NO}_2^-$  ion; the anionic exchange reduces the interlayer spacing, leading to higher 2-theta reflections. This has also been previously reported by Tedim et al. [15]. However, the 003 peaks in mild pH could also show an overlap of LDH- $\text{NO}_2^-$  and LDH- $\text{OH}^-$ , due to the possible parallel placement of  $\text{NO}_2^-$  in the interlayer. The  $\text{NO}_2^-$  ion placed inclined to the cationic layers will tend to show more layer contraction upon ion exchange with  $\text{OH}^-$  (Figure 7b). The parameter for cationic spacing ( $d_{110}$ ) in the brucite-like layer stays constant as the pH increases, signifying that only anionic exchange has occurred as external concentration of  $\text{OH}^-$  increased, and the cationic layer has stayed intact and unchanged.

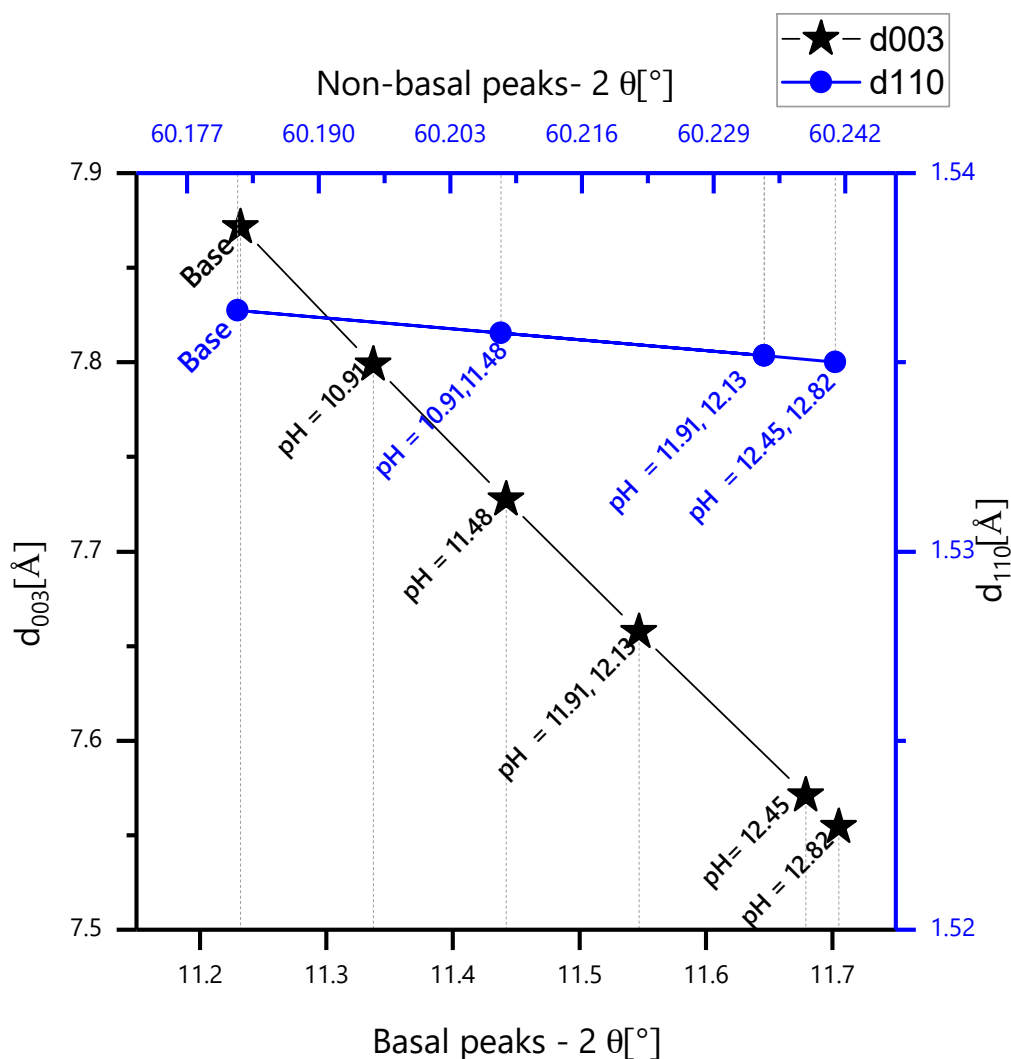


**Figure 8.** Shift of  $d_{003}$  and  $d_{110}$  as a function of pH.

These XRD peaks are also indicative of the structural stability in the high alkaline range. The partial dissolution of LDH starts around pH 12.5. The powders until this pH show characteristic peaks of the LDH, despite the shift in the intercalated anion, but from pH 12.5 onwards, new peaks are detected and attributed to  $\text{ZnO}$ ,  $\text{Zn}(\text{OH})_2$ ,  $\text{Al}_2\text{O}_3$ , etc.

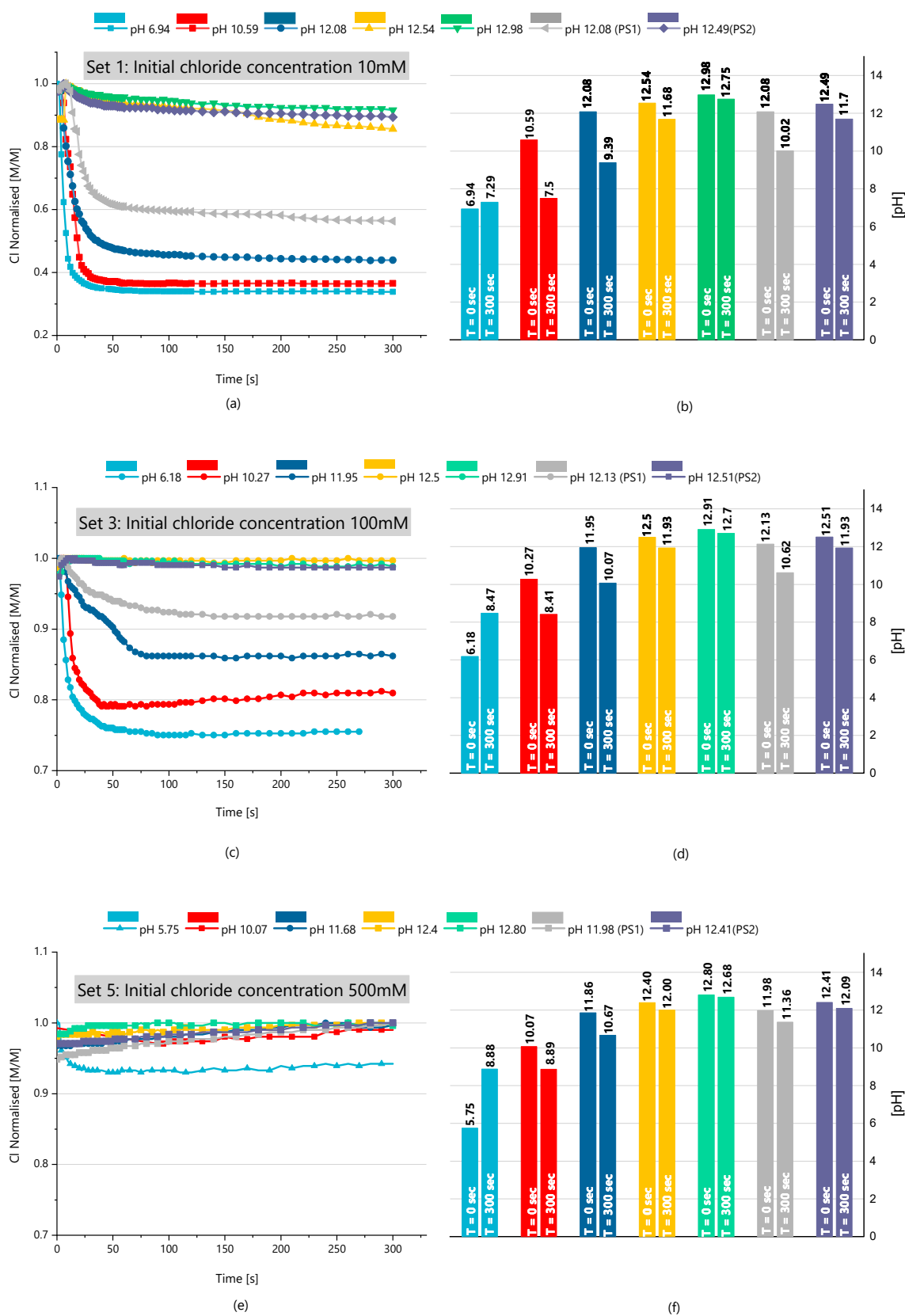
Finally, the XRD pattern of the small amount of solid that did not dissolve at pH 13.48 shows no peaks of the LDH (the LDH structure is lost) and is dominated by the peaks of oxides and hydroxides of Zn and Al, which were already visible in pH 12.45 and 12.82.

### 3.3. Chloride Entrapment and the Effect of pH

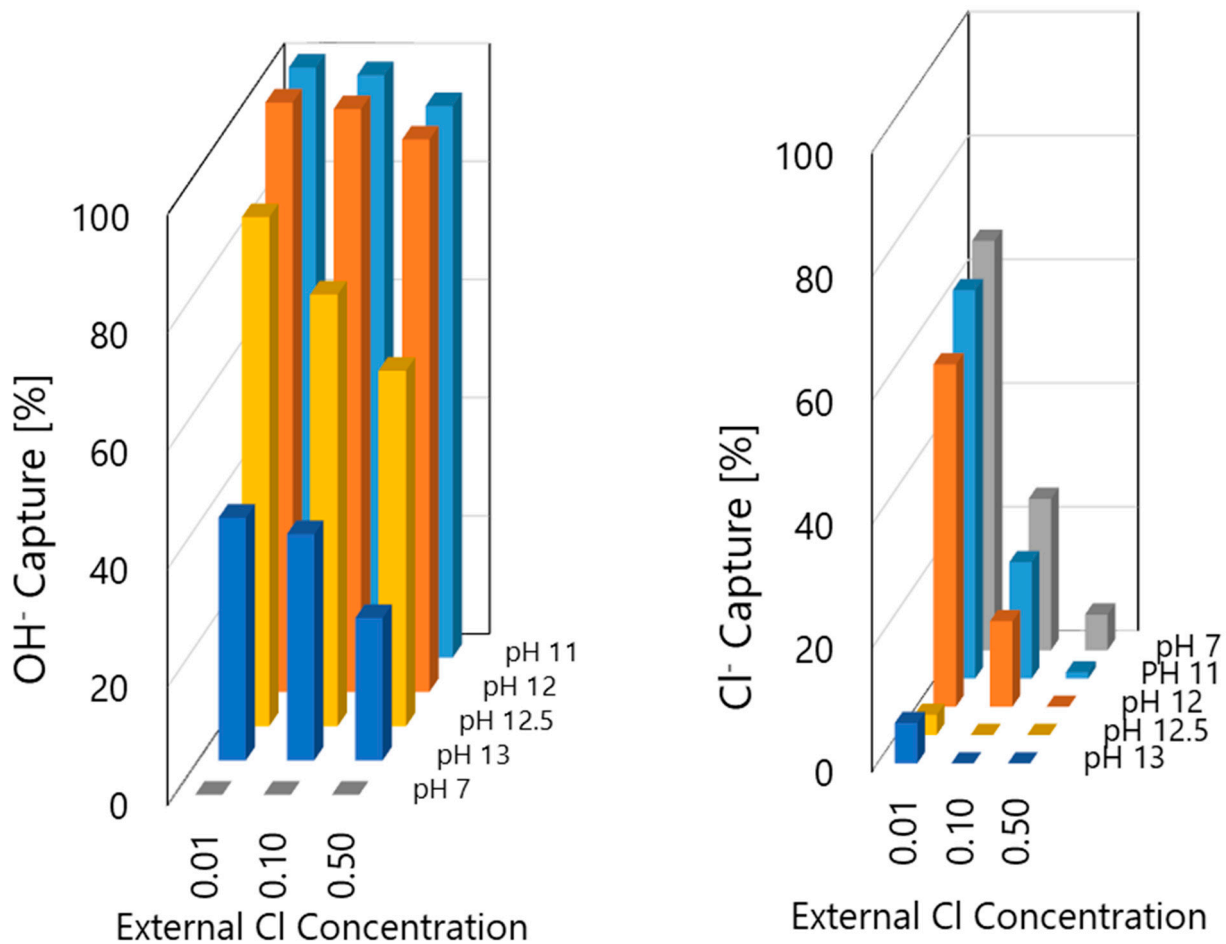
For the application of ZnAl-NO<sub>2</sub> as chloride-entrapping additive in cementitious environments, it is highly relevant to verify the Cl<sup>-</sup> binding capacity of this LDH in the presence of a high concentration of OH<sup>-</sup> ions. Therefore, the binding capacity of the LDH as a function of chloride concentration and pH was investigated. Representative results are presented in Figure 9, for starting NaCl solutions of 10, 100 and 500 mM with different pH values. The concentrations are plotted normalized, i.e., they appear divided by the starting concentration, for a better comparison of the changes in the different cases. These plots show the drop in chloride concentration after LDH was added to solution. The pH before and after the addition of LDH is also shown.

Figure 9a,b refer to the tests conducted with a starting chloride concentration of 10 mM at different pH. The highest chloride capture occurred at the lowest pH (6.94), where the concentration dropped to ~30 percent of the initial value. The process is very fast, taking less than 1 min to attain equilibrium. The Cl<sup>-</sup> capture at this pH (6.94) took place with a slight increase in the pH. This pH increase could be due to the release of OH<sup>-</sup> bound to the surface of the LDH or to a small dissolution of the LDH itself. In fact, the addition of 1 g of LDH to distilled water increased the pH and the conductivity of the solution, confirming that ions have passed from the LDH to solution. At pH 10.59, almost the same amount of chloride ions was captured, and it was accompanied by a decrease of pH from 10.59 to 7.5. This signifies that both Cl<sup>-</sup> and OH<sup>-</sup> were captured by the LDH. As the pH rises, so rises the amount of OH<sup>-</sup> that is captured, while the entrapment of chloride significantly decreases. Above pH 12, the amount of Cl<sup>-</sup> captured becomes very small.

A similar description applies for the other NaCl concentrations. The higher capture occurs in near-neutral solution, decreasing with the increase in pH, until it becomes almost negligible at a very high pH. However, it is noticeable that, for the same pH, the amount of OH<sup>-</sup> captured is smaller as the concentration of Cl<sup>-</sup> increases. The tendencies are better perceived in Figure 10. The ZnAl-NO<sub>2</sub> has higher selectivity to OH<sup>-</sup> than Cl<sup>-</sup>, and for a higher pH, it is captured preferentially with almost no Cl<sup>-</sup> captured. However, the capture of OH<sup>-</sup> is not so effective for a higher concentration of chloride. These results show that, in spite of the higher importance of selectivity, the concentration also counts. It is also evident that LDH leads to a decrease of pH of the surrounding solution, which can bring serious risks to the stability of the passive film on the rebar surface.



**Figure 9.** Results of the chloride-entrapment tests with the effect of pH. Plots on the left depict the change of chloride concentration (divided by the initial NaCl concentration) after LDH was added to solution. The graphs on the right show the solution pH before and after the addition of LDH. (a,b) Chloride ion and pH measurement in solutions at an initial chloride concentration of 10 mM, respectively. (c,d) Chloride ion and pH measurement in solutions at an initial chloride concentration of 100 mM, respectively. (e,f) Chloride ion and pH measurement in solutions, at an initial chloride concentration of 500 mM, respectively.



**Figure 10.** Comparison of the moles of  $\text{Cl}^-$  and  $\text{OH}^-$  captured, compared to the existing moles before the addition of LDH.

### 3.3.1. Effect of Time on the Chloride Entrapment

The entrapment tests described in the last section were conducted for just 300 s and did not continue, because the ionic exchange was quite fast after the addition of LDH, happening in less than 1 min, with the subsequent readings being stable. In any case, the samples were sealed for 15 days and then analyzed again, to look for any changes in  $\text{Cl}^-$  concentration and pH. As confirmed in Figure 11, with two representative examples, no significant changes were detected in both parameters measured after 300 s and 15 days. This confirms that the process is very fast, without further evolution.

The XRD analysis of two powders after 15-day exposure to alkaline solution, with and without NaCl, is presented in Figure 12. A clear shift of the 003 peak is seen for both the powders, as compared to the base material. The peaks of the powders exposed to just  $\text{OH}^-$  or to  $\text{OH}^-$  and  $\text{Cl}^-$  are quite close to each other and are not clearly distinguishable.

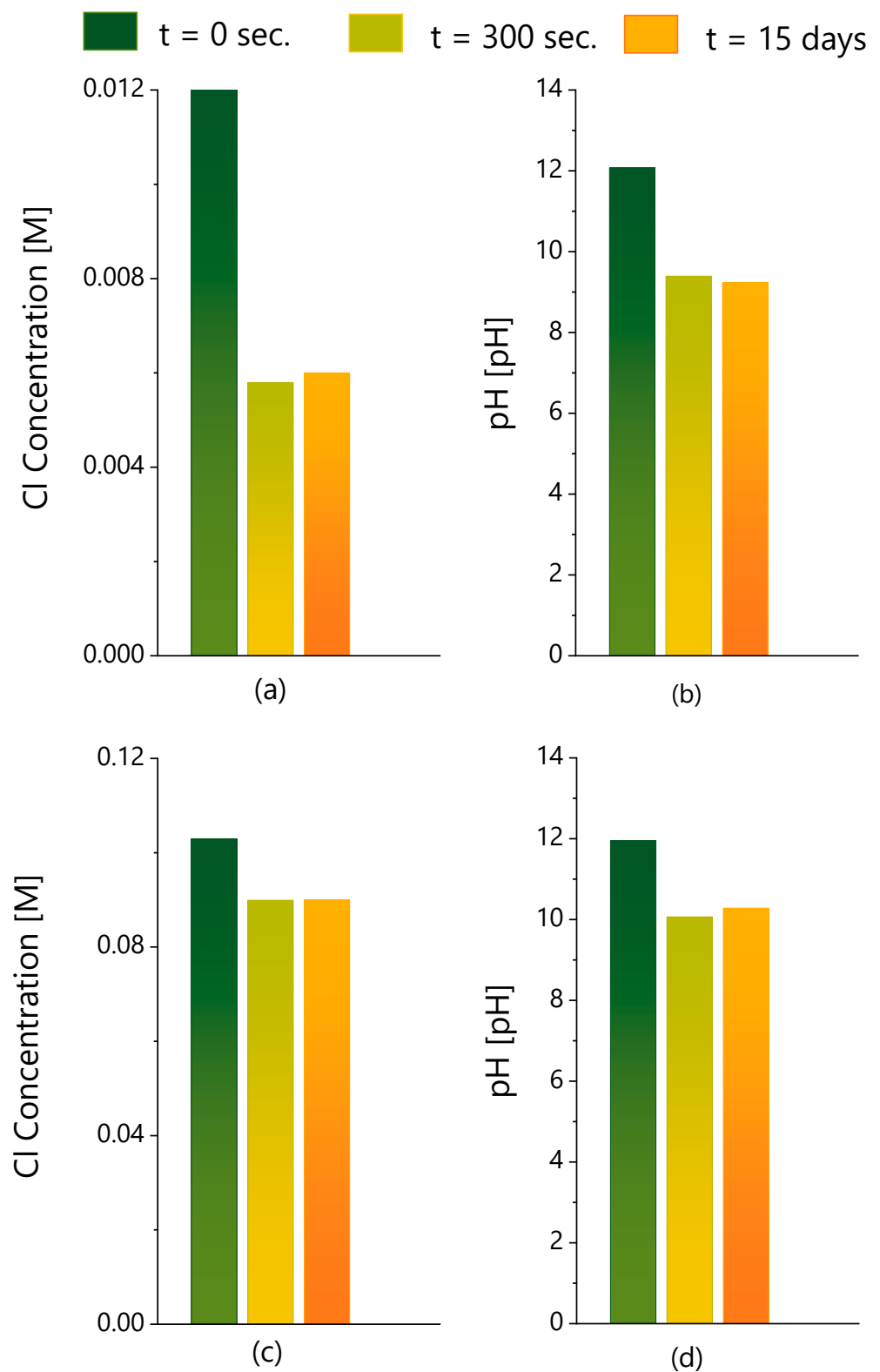


**Figure 11.** Long-term evaluation of chloride entrapment. (a) Cl<sup>-</sup> concentration and (b) pH of a 12 mM NaCl solution with initial pH = 12.08 measured before ( $t = 0$  s) and after (300 s and 15 days) the addition of LDH. (c,d) Similar measurements of a solution initially with 100 mM NaCl and pH 12.95.

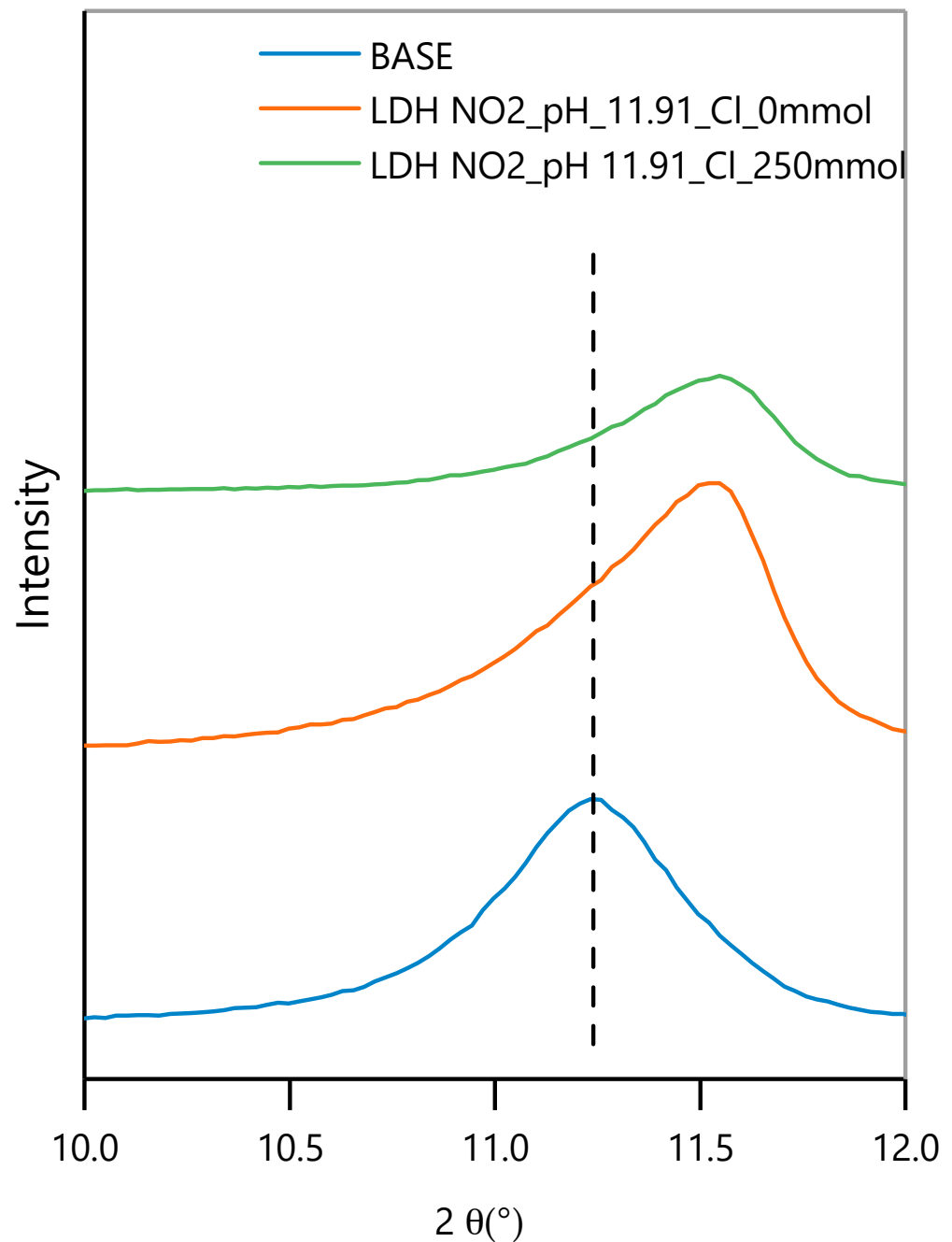


**Figure 12.** XRD plot detail of the 003 reflection of the LDH before tests (base) and the powder after 15 days of immersion in a solution with pH = 11.91, with and without 250 mM NaCl.

### 3.3.2. Chloride Binding Capacity

The chloride-binding capacity can be defined as the amount of chloride ion that is bound by a given mass of LDH. It can be expressed as the amount of  $\text{Cl}^-$  ion bound to LDH per unit mass of LDH at the onset of equilibrium. As such, the chloride-binding capacity represents a heterogeneous equilibrium between the  $\text{Cl}^-$  bound to LDH and the free  $\text{Cl}^-$  available in the solution. However, this equilibrium is sensitive to the pH of the environment and is explained later. The chloride-binding capacity can be determined by using the following formula [22,28]:

$$B_c = \frac{V_{sol} (C_0 - C_e) M_{Cl}}{m_{LDH}} \quad (1)$$

where  $B_c$  is the binding capacity (in mg/g),  $V_{sol}$  is the volume of solution (L),  $m_{LDH}$  is the mass of LDH added to the solution (g),  $C_0$  and  $C_e$  are the initial and equilibrium chloride concentrations (mM) and  $M_{Cl}$  is the molar mass of chloride. The binding (or loading) capacity of ZnAl-NO<sub>2</sub> for Cl<sup>-</sup> was calculated from the results of the chloride entrapment studies, using Equation (1), and is presented in Figure 13. The binding capacity increased with the Cl<sup>-</sup> concentration, up to a value where it then remained constant. The highest chloride loading was ~45 mg/g (1.28 mmol/g) and occurred at near neutral pH for the initial chloride concentration of 250 mM. The binding capacity is strongly dependent of the pH. At pH 12, it was half of the value in near-neutral pH, and above pH = 12.5, no substantial chloride was captured. The data for these equilibrium isotherms were obtained at room temperature (23 ± 1 °C). It is known that the loading capacity of Zn-Al-based LDH increases with temperature [36].

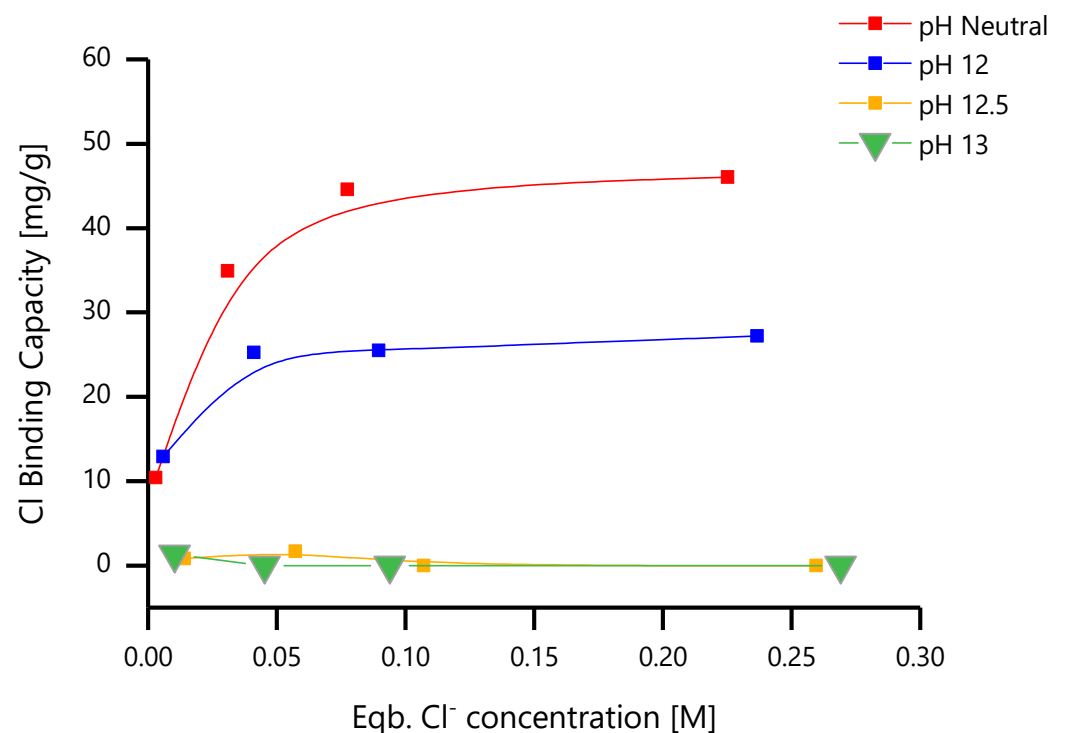


**Figure 13.** Chloride binding capacity of ZnAl-NO<sub>2</sub> in the alkaline pH range.

### 3.4. Compatibility with Cement

The experiments described so far were done in aqueous solution, with most of them at a high pH, to reflect the conditions inside cementitious materials. Naturally, the best approach is to test the LDH directly incorporated in these materials. It was decided to perform tests with mortars with 2% LDH with respect to cement. Before that, the compatibility of the ZnAl-NO<sub>2</sub> with cement was investigated (Figure 14). It was observed that addition of LDH had a retarding effect on the cement curing. The sample with LDH displayed a slow curing, as compared to the reference samples. Cement paste (w/c = 0.5) with 2 wt% LDH took a very long time to harden, that is, around 17 days, compared to one day of the reference sample (without LDH). It is well-known that zinc ions can retard the hydration process. Trezza [37] used IR, XPS and calorimetry to investigate the effect of Zn<sup>2+</sup> on the hydration processes and observed the delay of the cement hydration and attributed this to the formation of a new phase, Ca(Zn(OH)<sub>3</sub>)<sub>2</sub>·2H<sub>2</sub>O. Citing Asavapisit et al. [38], Trezza concluded that the formation of Ca-Zn complexes decreased the concentration of Ca<sup>2+</sup> ions required to form the CSH phase. The higher the concentration of Zn<sup>2+</sup>, the greater the quantity of the Ca-Zn phase and the longer the hydration time. Stephan et al. [39] also

concluded that formation of the Ca-Zn phase significantly retards the hydration process by reducing the concentration of  $\text{OH}^-$  and  $\text{Ca}^{2+}$  ions.

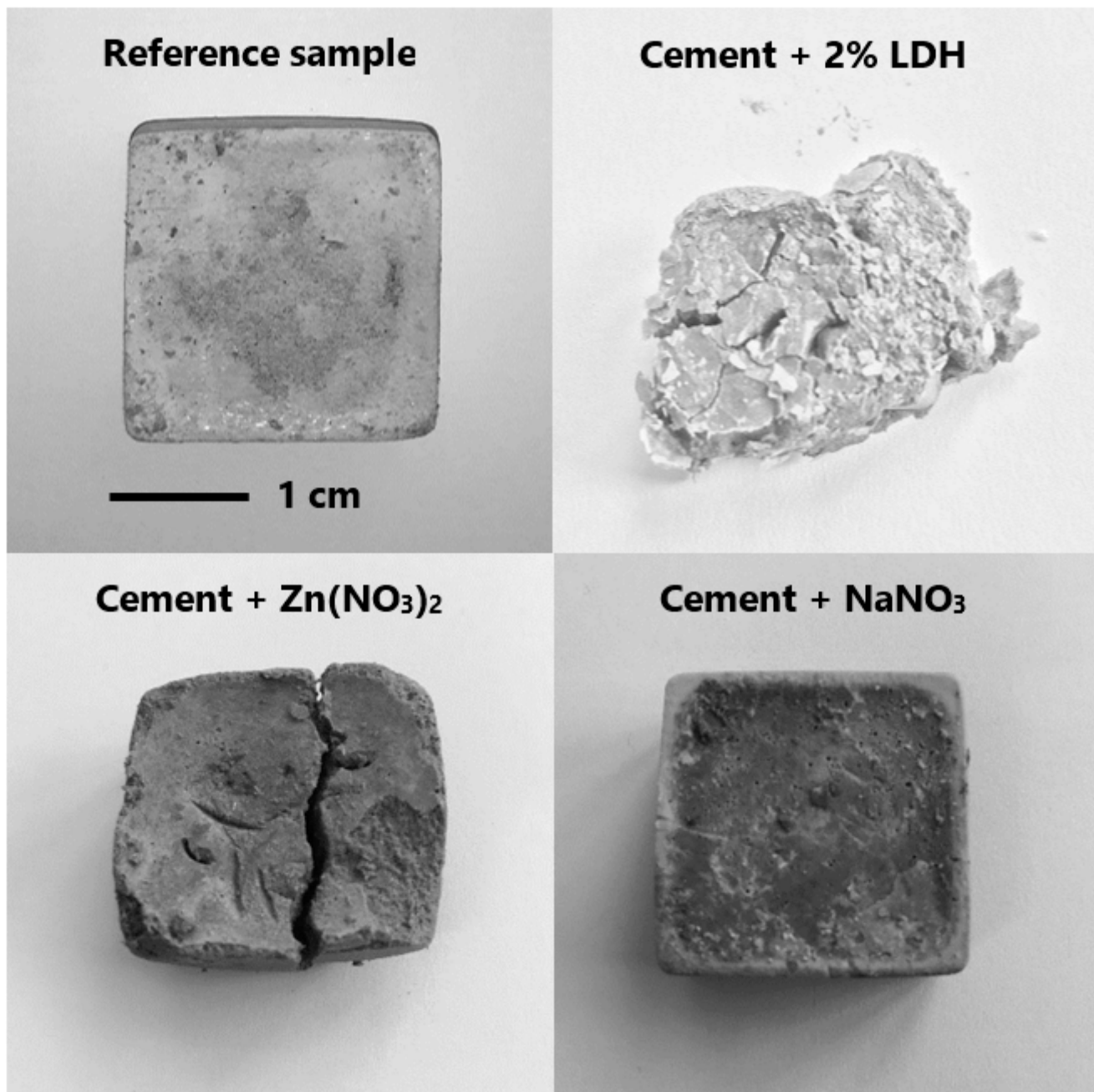


**Figure 14.** Compatibility of ZnAl-NO<sub>2</sub> with cement. Reference and cement + NaNO<sub>3</sub> samples harden in one day. Cement + ZnAlNO<sub>2</sub> or Zn(NO<sub>3</sub>)<sub>2</sub> took about 20 days to harden. ( $w/c = 0.5$ ).

To confirm that it was the  $\text{Zn}^{2+}$  from LDH dissolution that interfered with the curing, cement pastes were cast with Zn(NO<sub>3</sub>)<sub>2</sub>. Similar to specimens with LDH, the samples showed a clay-like behavior and took a long time to harden. To rule out the effect of  $\text{NO}_3^-$  on the hydration process, samples were cast with NaNO<sub>3</sub> with the same amount of  $\text{NO}_3^-$  as the samples with Zn(NO<sub>3</sub>)<sub>2</sub> as shown in Figure 14.  $\text{NO}_3^-$  ions are traditionally used as setting accelerators in concrete, usually in the form of Ca(NO<sub>3</sub>)<sub>2</sub> [40,41].

It is also important to note that the LDH particle size is a very important factor that should be taken into consideration. In a separate study from the authors [42], it was observed that a curing time similar to the reference samples was obtained when LDH

particles of mean size  $\sim 125 \mu\text{m}$  were used, instead of the  $\sim 25 \mu\text{m}$  used in the present study. Therefore, the authors acknowledge that particle size plays a crucial role as bigger LDH agglomerates can have a reduced exposed surface area, leading to a lower dissolution at high pH. The effect of the particle size of LDH on the properties on concrete, especially chloride ingress, has been documented in the studies by Qu et al. [43]. The results reported in this work are confined to only one particular particle size, i.e.,  $\sim 25 \mu\text{m}$ . For different particle sizes, reproducibility can be affected. Further studies are being planned to better characterize the effect of LDH and its particle sizes in cement paste hydration, and such studies will be reported in the future.

### 3.5. Embedded Sensors and Chloride Ingress in Mortar

To directly assess the effect of LDH on the transport of  $\text{Cl}^-$  inside cementitious materials, chloride sensors were cast in mortar samples, as described in Section 2.6. The mortars were immersed in 3.5% NaCl, and the potential of the sensors was measured, over time, against a reference electrode placed in the solution. From the chloride concentrations in the different positions of the mortar and at the different times, it was possible to plot the chloride profile inside the reference mortar and inside the mortar with  $\text{ZnAl-NO}_2$ , presented in Figure 15a,b respectively. In these plots, 0 cm corresponds to the surface of the mortar in contact with the solution, while the other values are the position of the sensors inside the mortar.

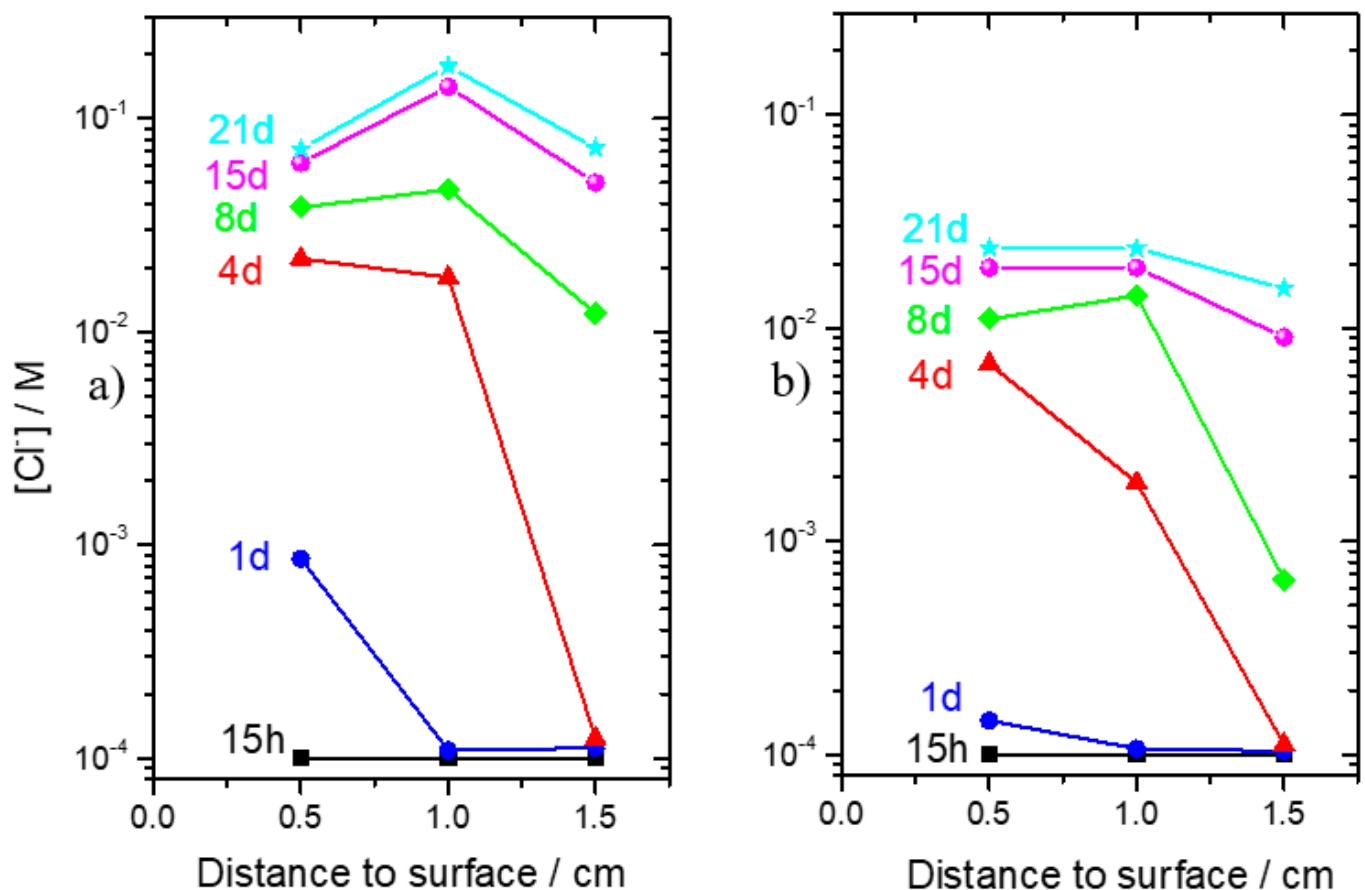


**Figure 15.** Studies conducted in mortars. (a) Chloride profile inside reference mortar and (b) chloride profile inside mortar with  $\text{ZnAl-NO}_2$ .

The chloride penetration was detected first by the sensors closer to the surface. Interestingly, with time, the peak chloride concentration was found not at the surface but 1 cm inside the mortar. This is a common observation [44–46] that has been attributed to a skin

effect, i.e., to a different composition of the surface layers, compared to the bulk, due to contact with the casting mold [44,45]. Other authors attributed this effect to the gradient of moisture in the first few layers of the sample [44], as well as to surface reactions of the surface with the exposure environment [46]. The fact that the sensors were able to capture the concentration peak is an indication of their good functioning. The most important observation in Figure 15 is the slower ingress of chloride in the mortar with LDH.

### 3.6. Corrosion of Steel Bar in Mortar with and without ZnAl-NO<sub>2</sub>

In a final set of tests, steel rebars were placed in mortars without and with LDH (2 wt%, with respect to cement, or 0.3 wt% with respect to the total mass of mortar). The samples were exposed to 3.5% NaCl, and the corrosion potential ( $E_{\text{corr}}$ ) and polarization resistance ( $R_p$ ) were monitored over time. The results are presented in Figure 16. The less negative  $E_{\text{corr}}$  and the higher  $R_p$  of the steel in mortars with LDH point to lower corrosion, compared to the reference samples. The presence of LDH in the mortar seems to play a positive role, which can be even more pronounced if a higher amount of LDH was present.

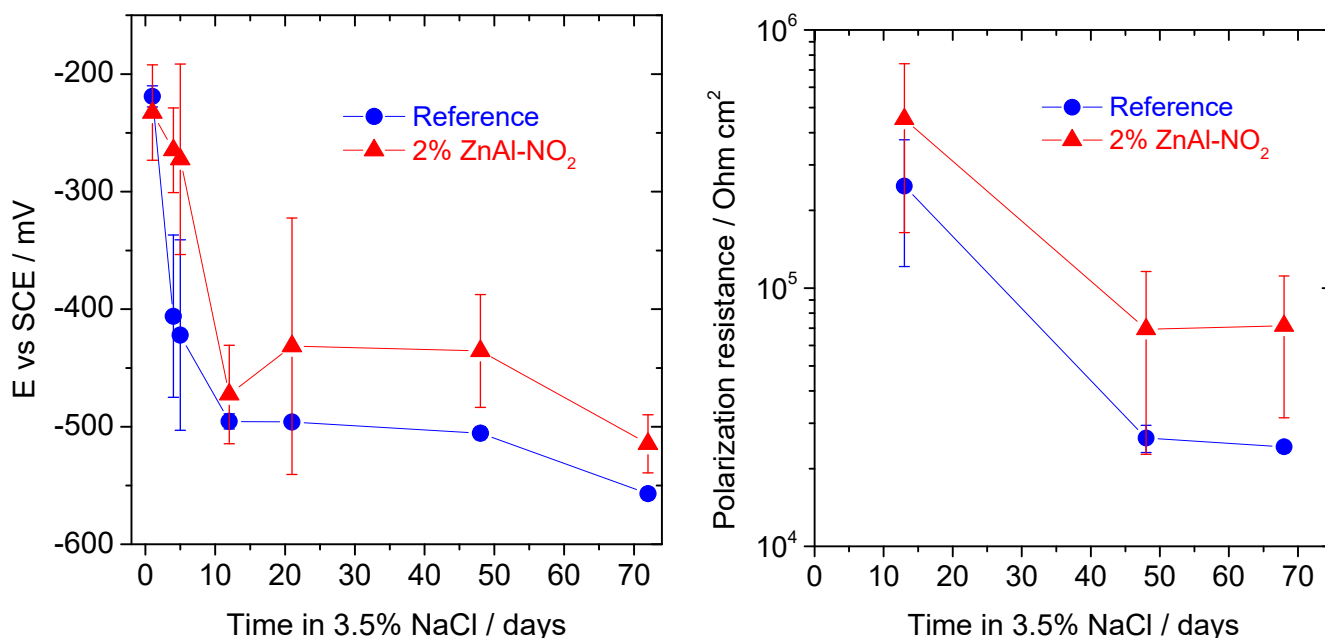


**Figure 16.** Corrosion potential and polarization resistance of steel rebar in mortars without and with 2 wt% (to cement fraction) ZnAl-NO<sub>2</sub> immersed in 3.5% NaCl.

The experiments with the LDH in mortars showed positive effects (lower ingress of chloride in mortar and higher corrosion resistance of steel), despite the low amount of LDH added (0.3 wt%) and the high porosity of the mortar. It is possible that the dissolution of LDH releases aluminum ions, which will promote the formation of more AFm phases (family of hydrated calcium aluminates) during cement hydration. This has been previously demonstrated by the authors, in a separate study, where the formation of AFm was recently confirmed by using in situ XRD on hydrating cement pastes with 2% Mg-based LDH. The reader is directed to Mir et al. [27], for detailed information on this effect. The dissolution of LDH leads to the formation of extra quantities of AFm which can chemically bind chloride ions. The extra amount of AFm phases can thus lead to additional chemical binding of chloride ions by forming Friedel's salt and Kuzel's salt and is also reported in the studies by Chen et al. [47]. Additionally, the filler effect of remaining undissolved LDH particles can play a positive role in chloride ingress by making the microstructure more tortuous, without decreasing the total porosity [43]. The higher corrosion resistance of steel in the mortar that contains LDH can be simply due to the release of NO<sub>2</sub><sup>-</sup> to the pore solution, as a result of the LDH dissolution and ion exchange with OH<sup>-</sup> on the remaining powder. This

contrast between the results with LDH in solution and in mortar needs more investigation, and additional studies are planned for the future.

These results with mortars are still preliminary because the experiments were performed with a limited number of replicate specimens (three of each type), in porous mortar (to accelerate the ion transport process), and the amount of LDH was only 0.3 wt% to the total mass of the mortar. Work is being performed with a higher number of samples, with better quality mortar, higher amounts of LDH and longer testing times in the mortar, in order to better understand the behavior of the LDH inside mortars, and will be reported in the future.

#### 4. Conclusions

Based on the discussion presented in this work, the following conclusions can be drawn.

1. The Zn-Al LDH presents very good chloride-capture capability in near-neutral pH. Our investigations reported a peak binding capacity of about ~45 mg of Cl per gram of LDH. However, as the pH increases, the chloride-capture capability of Zn-Al LDH is reduced.
2. The LDH is stable in alkaline medium, until pH ~12.5. Partial dissolution occurs at a higher pH, with the release of the constituent anions ( $\text{Zn}^{2+}$ ,  $\text{Al}^{3+}$ ,  $\text{NO}_2^-$ ) to the environment.
3. The ZnAl- $\text{NO}_2$  delays the hardening of cement paste and mortars. This has been attributed to the zinc ions released by the partial LDH dissolution which interfere with the cement hydration reaction.
4. The partial dissolution and preferential capture of  $\text{OH}^-$  at the pH values typical of cementitious material suggest the inadequacy of ZnAl- $\text{NO}_2$  for the chloride capture inside concrete, where a pH higher than 13 is possible.
5. Mortars with the LDH presented a slower penetration of  $\text{Cl}^-$  ions and led to higher corrosion resistance of the embedded steel rebar, even with a small amount (0.3% of total mass of mortar). Earlier studies pointed out that LDH dissolution can possibly lead to higher amounts of AFm being generated. However, additional experiments are needed to clarify this effect for ZnAl LDH. As a future scope to this work, more work will be performed to investigate the dissolution and working mechanism of LDH in concrete and will be reported in future.

**Author Contributions:** Conceptualization, Z.M.M., C.G. and A.C.B.; formal analysis, Z.M.M., C.G., A.C.B., R.S., F.M. and C.R.; investigation, Z.M.M., C.G. and A.C.B.; resources, F.M. and C.R.; supervision, A.C.B., F.M., C.R., J.T., D.H., M.G.S.F. and M.L.Z.; writing—original draft, Z.M.M. and A.C.B.; writing—review and editing, A.C.B. and M.L.Z. All authors have read and agreed to the published version of the manuscript.

**Funding:** This research was funded by the HORIZON 2020 collaborative project “LORCENIS” (Long Lasting Reinforced Concrete for Energy Infrastructure under Severe Operating Conditions, Grant agreement n° 685445), the European Union’s COST Action (SARCOS, Self-healing As preventive Repair of Concrete Structures), under grant agreement No. CA15202, and in the scope of the project CICECO—Aveiro Institute of Materials, POCI-01-0145-FEDER-007679 (FCT Reference UID/CTM/50011/2013). AB acknowledges FCT—Fundação para a Ciência e a Tecnologia, I.P., in the scope of the framework contract foreseen in the numbers 4, 5 and 6 of the article 23, of the Decree-Law 57/2016, of 29 August, changed by Law 57/2017, as of 19 July.

**Data Availability Statement:** The authors declare that the data presented in this work are available within the article. Extra data could be requested from the corresponding author.

**Conflicts of Interest:** The authors declare no conflict of interest. The funders had no role in the design of the study; in the collection, analyses or interpretation of data; in the writing of the manuscript; or in the decision to publish the results.

## References

1. Page, C.L. Mechanism of Corrosion Protection in Reinforced-Concrete Marine Structures. *Nature* **1975**, *258*, 514–515. [[CrossRef](#)]
2. Tuutti, K. *Corrosion of Steel in Concrete. Technical Report*; Swedish Cement and Concrete Research Institute: Stockholm, Sweden, 1982.
3. Bertolini, L.; Elsener, B.; Pedferri, P.; Redaelli, E.; Polder, R. *Corrosion of Steel in Concrete: Prevention, Diagnosis, Repair*; Wiley: Hoboken, NJ, USA, 2013.
4. Angst, U. Challenges and Opportunities in Corrosion of Steel in Concrete. *Mater. Struct.* **2018**, *51*, 1–20. [[CrossRef](#)]
5. Lian, C.; Zhuge, Y.; Beecham, S. The Relationship between Porosity and Strength for Porous Concrete. *Constr. Build. Mater.* **2011**, *25*, 4294–4298. [[CrossRef](#)]
6. Alonso, C.; Andrade, C.; Castellote, M.; Castro, P. Chloride Threshold Values to Depassivate Reinforcing Bars Embedded in a Standardized Opc Mortar. *Cem. Concr. Res.* **2007**, *30*, 1047–1055. [[CrossRef](#)]
7. Ghods, P.; Isgor, O.B.; McRae, G.A.; Li, J.; Gu, G.P. Microscopic Investigation of Mill Scale and Its Proposed Effect on the Variability of Chloride-Induced Depassivation of Carbon Steel Rebar. *Corros. Sci.* **2011**, *53*, 946–954. [[CrossRef](#)]
8. Mir, M.Z.; Bastos, A.; Höche, D.; Zheludkevich, M.L. Recent Advances on the Application of Layered Double Hydroxides in Concrete—A Review. *Materials* **2020**, *13*, 1426. [[CrossRef](#)]
9. Li, F.; Duan, X. Applications of Layered Double Hydroxides. In *Layered Double Hydroxides*; Duan, X., David, E.G., Eds.; Springer: Berlin/Heidelberg, Germany, 2006.
10. Peng, C.; Yu, J.Y.; Zhao, Z.J.; Dai, J.; Fu, J.Y.; Zhao, M.L.; Wang, W. Synthesis and Properties of a Clean and Sustainable Deicing Additive for Asphalt Mixture. *PLoS ONE* **2015**, *10*, e0115721. [[CrossRef](#)] [[PubMed](#)]
11. Kirm, I.; Francesc, M.; Xavier, R.; Cesteros, Y.; Salagre, P.; Sueiras, J. Epoxidation of Styrene with Hydrogen Peroxide Using Hydrotalcites as Heterogeneous Catalysts. *Appl. Catalysis A General* **2004**, *272*, 175–185. [[CrossRef](#)]
12. Park, D.H.; Choi, G.; Choy, J.H. Bio-Layered Double Hydroxides Nanohybrids for Theranostics Applications. In *Photofunctional Layered Materials*; Dongpeng, Y., Min, W., Eds.; Springer International Publishing: Cham, Switzerland, 2015.
13. Ogawa, M.; Kazuyuki, K. Photofunctions of Intercalation Compounds. *Chem. Rev.* **1995**, *15*, 399–438. [[CrossRef](#)]
14. Liao, C.-S.; Wei-Bin, Y. Structure and Conductive Properties of Poly (Ethylene Oxide)/Layered Double Hydroxide Nanocomposite Polymer Electrolytes. *Electrochim. Acta* **2004**, *49*, 4993–4998. [[CrossRef](#)]
15. Tedim, J.; Kuznetsova, A.; Salak, A.N.; Montemor, F.; Snihirova, D.; Pilz, M.; Zheludkevich, M.L.; Ferreira, M.G.S. Zn-Al Layered Double Hydroxides as Chloride Nanotraps in Active Protective Coatings. *Corros. Sci.* **2012**, *55*, 1–4. [[CrossRef](#)]
16. Choy, J.H.; Kwak, S.Y.; Park, J.S.; Jeong, Y.J.; Portier, J. Intercalative Nanohybrids of Nucleoside Monophosphates and DNA in Layered Metal Hydroxide. *J. Am. Chem. Soc.* **1999**, *121*, 1399–1400. [[CrossRef](#)]
17. Martin, K.J.; Thomas, J.P. Layered Double Hydroxides as Supported Anionic Reagents. Halide-Ion Reactivity in Zinc Chromium Hexahydroxide Halide Hydrates  $[Zn_2Cr(OH)_6 \cdot nNH_2O](X = Cl, I)$ . *J. Am. Chem. Soc.* **1986**, *108*, 541–542. [[CrossRef](#)] [[PubMed](#)]
18. Crepaldi, E.L.; Paulo, C.P.; João, B.V. Comparative Study of the Coprecipitation Methods for the Preparation of Layered Double Hydroxides. *J. Braz. Chem. Soc.* **2000**, *11*, 64–70. [[CrossRef](#)]
19. He, J.; Min, W.; Bo, L.; Yu, K.; David, G.E.; Duan, X. Preparation of Layered Double Hydroxides. In *Layered Double Hydroxides*; Duan, X., David, G.E., Eds.; Springer: Berlin/Heidelberg, Germany, 2006.
20. Costa, D.G.; Rocha, A.B.; Souza, W.F.; Chiaro, S.S.X.; Leitão, A.A. Comparative Structural, Thermodynamic and Electronic Analyses of Znalán–Hydrotalcite-Like Compounds (an–Cl–, F–, Br–, OH–, CO<sub>3</sub><sup>2–</sup> or NO<sub>3</sub><sup>–</sup>): An Ab Initio Study. *Appl. Clay Sci.* **2012**, *56*, 16–22. [[CrossRef](#)]
21. Hibino, T. Anion Selectivity of Layered Double Hydroxides: Effects of Crystallinity and Charge Density. *Eur. J. Inorg. Chem.* **2018**, *6*, 722–730. [[CrossRef](#)]
22. Zuo, J.D.; Wu, B.; Luo, C.Y.; Dong, B.Q.; Xing, F. Preparation of MgAl Layered Double Hydroxides Intercalated with Nitrite Ions and Corrosion Protection of Steel Bars in Simulated Carbonated Concrete Pore Solution. *Corros. Sci.* **2019**, *152*, 120–129. [[CrossRef](#)]
23. Raki, L.; Beaudoin, J.J.; Mitchell, L. Layered Double Hydroxide-Like Materials: Nanocomposites for Use in Concrete. *Cem. Concr. Res.* **2004**, *34*, 1717–1724. [[CrossRef](#)]
24. Xu, S.; Chen, Z.; Zhang, B.; Yu, J.; Zhang, F.; Evans, D.G. Facile Preparation of Pure CaAl-Layered Double Hydroxides and Their Application as a Hardening Accelerator in Concrete. *Chem. Eng. J.* **2009**, *155*, 881–885. [[CrossRef](#)]
25. Shui, Z.; Juntao, M.; Wei, C.; Xiaoxing, C. Chloride Binding Capacity of Cement Paste Containing Layered Double Hydroxide (Ldh). *J. Test. Eval.* **2012**, *40*, 796–800.
26. Duan, P.; Chen, W.; Ma, J.; Shui, Z. Influence of Layered Double Hydroxides on Microstructure and Carbonation Resistance of Sulphoaluminate Cement Concrete. *Constr. Build. Mater.* **2013**, *48*, 601–609.
27. Mir, Z.M.; Alexandre, B.; Celestino, G.; Urs, M.; Alonso, M.C.; Villar, K.; Miguel, P.; Rabade, F.M.; Cláudia, M.; Rocha, P.M.; et al. Numerical and Experimental Analysis of Self-Protection in Reinforced Concrete Due to Application of Mg–Al–No<sub>2</sub> Layered Double Hydroxides. *Adv. Eng. Mater.* **2020**, *22*, 2000398. [[CrossRef](#)]
28. Chen, Y.X.; Shui, Z.H.; Chen, W.; Chen, G.W. Chloride Binding of Synthetic Ca–Al–No<sub>3</sub> Ldhs in Hardened Cement Paste. *Constr. Build. Mater.* **2015**, *93*, 1051–1058. [[CrossRef](#)]
29. Yoon, S.; Moon, J.; Bae, S.; Duan, X.N.; Giannelis, E.P.; Monteiro, P.M. Chloride Adsorption by Calcined Layered Double Hydroxides in Hardened Portland Cement Paste. *Mater. Chem. Phys.* **2014**, *145*, 376–386. [[CrossRef](#)]

30. Yang, Z.; Fischer, H.; Polder, R. Modified Hydrotalcites as a New Emerging Class of Smart Additive of Reinforced Concrete for Anticorrosion Applications: A Literature Review. *Mater. Corros. Werkst. Korros.* **2013**, *64*, 1066–1074. [[CrossRef](#)]
31. Tian, Y.W.; Dong, C.F.; Wang, G.; Cheng, X.Q.; Li, X.G. Zn-Al-No<sub>2</sub> Layered Double Hydroxide as a Controlled-Release Corrosion Inhibitor for Steel Reinforcements. *Mater. Lett.* **2019**, *236*, 517–520. [[CrossRef](#)]
32. SINTEF. *Norway European Union's Project, Lorcenis—Long Lasting Reinforced Concrete for Energy Infrastructure under Severe Operating Conditions, European Union Horizon 2020 Programme*; SINTEF: Trondheim, Norway, 2016–2020.
33. Poznyak, S.K.; Tedim, J.; Rodrigues, L.M.; Salak, A.N.; Zheludkevich, M.L.; Dick, L.F.P.; Ferreira, M.G.S. Novel Inorganic Host Layered Double Hydroxides Intercalated with Guest Organic Inhibitors for Anticorrosion Applications. *ACS Appl. Mater. Interfaces* **2009**, *1*, 2353–2362. [[CrossRef](#)]
34. Cao, Y.H.; Dong, S.G.; Zheng, D.J.; Wang, J.J.; Zhang, X.J.; Du, R.G.; Song, G.L.; Lin, C.J. Multifunctional Inhibition Based on Layered Double Hydroxides to Comprehensively Control Corrosion of Carbon Steel in Concrete. *Corros. Sci.* **2017**, *126*, 166–179. [[CrossRef](#)]
35. Ewald, P.P. William Henry Bragg and the New Crystallography. *Nature* **1962**, *195*, 320–325. [[CrossRef](#)]
36. Lv, L.; Sun, P.; Gu, Z.; Du, H.; Pang, X.; Tao, X.; Xu, R.; Xu, L. Removal of Chloride Ion from Aqueous Solution by ZnAl-No(3) Layered Double Hydroxides as Anion-Exchanger. *J. Hazard. Mater.* **2009**, *161*, 1444–1449. [[CrossRef](#)]
37. Trezza, M.A. Hydration Study of Ordinary Portland Cement in the Presence of Zinc Ions. *Mater. Res.* **2007**, *10*, 331–334. [[CrossRef](#)]
38. Asavapisit, S.; Fowler, G.; Cheeseman, C.R. Solution Chemistry During Cement Hydration in the Presence of Metal Hydroxide Wastes. *Cem. Concr. Res.* **1997**, *17*, 1249–1260. [[CrossRef](#)]
39. Stephan, D.H.; Maleki, D.K.; Eber, B.; Hårdtl, R. Influence of Cr, Ni, and Zn on the Properties of Pure Clinker Phases: Part, I. C3s. *Cem. Concr. Res.* **1999**, *29*, 545–552. [[CrossRef](#)]
40. Franke, W.; Magdalena, B.-S.; Tandre, O.; Gaurav, S. The Fate of Nitrate Ions in Concrete under the Focus of Corrosion Inhibition. In Proceedings of the 2nd International Conference on Durability of Concrete Structures, ICDCS 2010, Sapporo, Japan, 24–26 November 2010.
41. Justnes, H.; Nygaard, E.C. Technical Calcium Nitrate as Set Accelerator for Cement at Low Temperatures. *Cem. Concr. Res.* **1995**, *25*, 1766–1774.
42. Gomes, G.; Mir, Z.; Sampaio, R.; Bastos, A.; Tedim, J.; Maia, F.; Rocha, C.; Ferreira, M. Use of ZnAl-Layered Double Hydroxide (Ldh) to Extend the Service Life of Reinforced Concrete. *Materials* **2020**, *13*, 1769.
43. Qu, Z.Y.; Yu, Q.L.; Brouwers, H.J.H. Relationship between the Particle Size and Dosage of Ldhs and Concrete Resistance against Chloride Ingress. *Cem. Concr. Res.* **2018**, *105*, 81–90. [[CrossRef](#)]
44. Andrade, C.; Diez, L.M.; Alonso, C. Mathematical Modeling of a Concrete Surface “Skin Effect” on Diffusion in Chloride Contaminated Media. *Adv. Cem. Based Mater.* **1997**, *6*, 39–44. [[CrossRef](#)]
45. Castro, P.; de Rincon, O.T.; Pazini, E.J. Interpretation of Chloride Profiles from Concrete Exposed to Tropical Marine Environments. *Cem. Concr. Res.* **2001**, *31*, 529–537. [[CrossRef](#)]
46. De Weerd, K.; Orsáková, D.; Müller, A.C.A.; Larsen, C.K.; Pedersen, B.; Geiker, M.R. Towards the Understanding of Chloride Profiles in Marine Exposed Concrete, Impact of Leaching and Moisture Content. *Constr. Build. Mater.* **2016**, *120*, 418–431. [[CrossRef](#)]
47. Chen, P.; Ma, B.; Tan, H.; Liu, X.; Zhang, T.; Qi, H.; Peng, Y.; Yang, Q.; Wang, J. Effects of Amorphous Aluminum Hydroxide on Chloride Immobilization in Cement-Based Materials. *Constr. Build. Mater.* **2020**, *231*, 117171.